Research article

Biomedical Chromatography

Received: 18 October 2012, Revised: 21 November 2012, Accepted: 27 November 2012 Published online in Wiley Online Library: 24 January 2013

(wileyonlinelibrary.com) DOI 10.1002/bmc.2860

In vitro metabolism study of *Strychnos* alkaloids using high-performance liquid chromatography combined with hybrid ion trap/time-of-flight mass spectrometry

Ji-Xin Tian[a], Can Peng[a], Lei Xu[a], Yuan Tian[a] and Zun-Jian Zhang[a,b]*

ABSTRACT: In this report, the *in vitro* metabolism of *Strychnos* alkaloids was investigated using liquid chromatography/high-resolution mass spectrometry for the first time. Strychnine and brucine were selected as model compounds to determine the universal biotransformations of the *Strychnos* alkaloids in rat liver microsomes. The incubation mixtures were separated by a bidentate-C_{18} column, and then analyzed by on-line ion trap/time-of-flight mass spectrometry. With the assistance of mass defect filtering technique, full-scan accurate mass datasets were processed for the discovery of the related metabolites. The structural elucidations of these metabolites were achieved by comparing the changes in accurate molecular masses, calculating chemical component using Formula Predictor software and defining sites of biotransformation based upon accurate MS^n spectral information. As a result, 31 metabolites were identified, of which 26 metabolites were reported for the first time. These biotransformations included hydroxylation, *N*-oxidation, epoxidation, methylation, dehydrogenation, de-methoxylation, *O*-demethylation, as well as hydrolysis reactions. Copyright © 2013 John Wiley & Sons, Ltd.

Keywords: *Strychnos* alkaloids; *in vitro* metabolism; ion trap/time-of-flight mass spectrometer; mass defect filter

Introduction

The plants of *Strychnos* species have been used for centuries as herbal medicines in Asian countries. The dried seeds of *Strychnos nux-vomica* L. have been widely used as the key ingredient in many Indian traditional medicines (Ayurveda) or Chinese pharmaceutical preparations (Oudhia, 2008).

Strychnos alkaloids (SAs), a class of dihydroindole-type alkaloids, are believed to be the major bioactive compounds of various *Strychnos* species. The most commonly studied SAs are strychnine and brucine (chemical structures shown in Fig. 1), which are reported to possess anticancer (Deng *et al*., 2006; Agrawal *et al*., 2011), anti-arrhythmia (Yuan *et al*., 2011), anti-inflammatory and analgesic activities (Yin *et al*., 2003). On the other hand, SAs have also been reported to be responsible for side effects caused by their potential toxicities (Wang *et al*., 2004).

In vitro metabolism of strychnine was investigated from the mid-1980s until the early 1990s, leading to eight metabolites being discovered, such as strychnine 21,22-epoxide (Mishima *et al*., 1985), 16-hydroxystrychnine (Tanimoto *et al*., 1990) and 22-hydroxystrychnine (Tanimoto *et al*., 1991). In these studies, the metabolites were isolated from biological matrices and then characterized by means of UV, nuclear magnetic resonance (NMR) and mass spectrometries. However, low-abundance metabolites may be neglected using these approaches because of the overlapping signals from high-concentration metabolites. As a result, the complex metabolic behaviors of SAs *in vitro* remain unclear.

The inherently high selectivity and sensitivity of liquid chromatography/mass spectrometry (LC/MS) makes it the major analytical platform of choice for the identification of traces of metabolites in biological matrices (Prasad *et al*., 2011). In particular, LC combined with hybrid ion trap/time-of-flight mass spectrometry (LC/MS-IT-TOF) is useful for the characterization and identification of unknown metabolites as it can not only provide multistage fragmentations, but also determine the precise mass/charge ratios and thus the structures of product ions.

The present study represents the first investigation of *in vitro* metabolism of SAs using high-resolution LC/MS-IT-TOF. A metabolite identification workflow based on the integration of LC/MS-IT-TOF with mass defect filter (MDF) technique was developed for characterizing the major-to-trace metabolites of two SAs, namely strychnine and its dimethoxylated derivative brucine. At the same time, their universal biotransformation sites were summarized, which is necessary to better understand the pharmacological and toxicological activities of SA-containing herbal medicines.

* Correspondence to: Zun-Jian Zhang, Key Laboratory of Drug Quality Control and Pharmacovigilance (China Pharmaceutical University), Ministry of Education, Nanjing 210009, China. E-mail: zunjianzhangcpu@hotmail.com

[a] Key Laboratory of Drug Quality Control and Pharmacovigilance (China Pharmaceutical University), Ministry of Education, Nanjing 210009, China

[b] State Key Laboratory of Natural Medicines (China Pharmaceutical University), Nanjing 210009, China

Abbreviations used: CE, collision energ; ESI, electrospray ionization; MDF, mass defect filter; SA, *Strychnos* alkaloid.

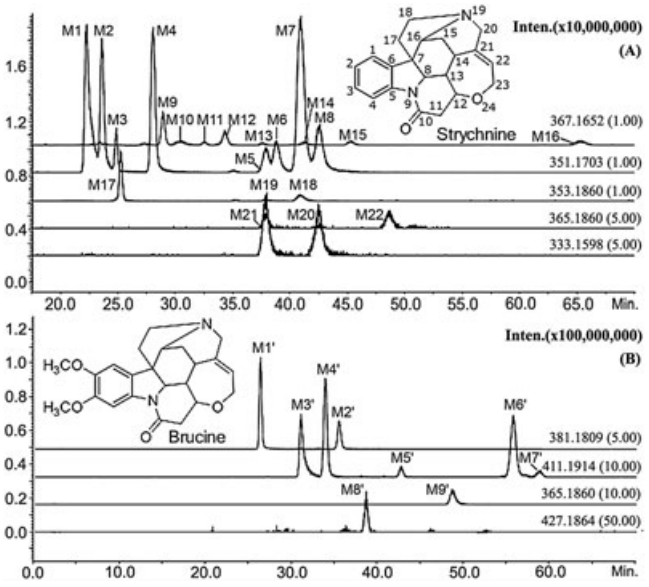

Figure 1. Extracted ion chromatograms of the metabolites of (A) strychnine and (B) brucine in rat liver microsomal incubation mixture. The structures of the parent compounds are shown in the inset.

Experimental and methods

Materials and reagents

Strychnine ($C_{21}H_{22}N_2O_2$, M_r 334.1681) and brucine ($C_{23}H_{26}N_2O_4$, M_r 394.1893) were purchased from the National Institute for the Control of Pharmaceutical and Biological Products (Beijing, China). Glucose-6-phosphate, yeast glucose-6-phosphate dehydrogenase and β-nicotinamide adenine dinucleotide phosphate disodium salt (β-NADP Na_2) were supplied by Sigma (St Louis, MO, USA). Methanol (HPLC-grade) was obtained from Merk (Darmstadt, Germany). Twice-distilled water was used throughout the study. All other chemicals were of analytical grade.

Preparation of rat liver microsomes

Sprague–Dawley rats (male, 180–210 g) were acclimatized for one week under standardized temperature (26 °C) and 12 h light/dark cycle environment with free access to standard food and water. After fasting for 12 h, rats were sacrificed by decapitation. The pooled livers were removed and washed immediately three times with ice-cold 0.15 M KCl, followed by homogenization with 2 volumes of 0.1 M potassium phosphate buffer (pH 7.4, containing 1.15% KCl). The homogenate was centrifuged at 9000 ***g*** for 20 min, and the supernatant was centrifuged again at 100,000 ***g*** for 60 min. The microsomal pellets were then suspended in 0.1 M potassium phosphate buffer (pH 7.4, containing 25% glycerol), and immediately stored at −80 °C. Microsomal protein concentration was determined by the method of Bradford (1976) using bovine serum albumin as the standard.

In vitro microsomal incubations

Strychnine or brucine (100 μM) was incubated in 200.0 μL of 0.1 M potassium phosphate buffer, pH 7.4, containing 1.0 mg protein/mL of rat liver microsomes, 1.0 mM β-$NADP^+$, 10.0 mM magnesium chloride, 10.0 mM glucose 6-phosphate and 1 U/mL yeast glucose-6-phosphate dehydrogenase at 37 °C for 1 h. As controls, the incubation mixture without β-$NADP^+$ were analyzed. Each of the mixtures was extracted with 600.0 μL of methanol and centrifuged at 14,000 ***g*** for 10 min. The supernatant was separated and evaporated under a gentle stream of nitrogen. The residue from each extract was redissolved in 80.0 μL of methanol and passed through a 0.22 μm membrane filter; 5.0 μL of the resulted aliquot was injected for LC analysis.

LC/MS-IT-TOF analysis

The LC experiments were conducted on a Shimadzu (Kyoto, Japan) LC system consisting of an LC-30 AD binary pump, a SIL-30 AC autosampler and a CTO-20 AC column oven. The chromatographic separation was carried out on an Agilent Zorbax Extend-C_{18} column (4.6 mm i.d. × 150 mm, 5 μm) under the gradient elution mode. The mobile phase was a mixture of 10 mM CH_3COONH_4 (pH3.0, A) and methanol (B). The linear gradient was programmed as follows: initial, A:B 95:5, v/v; 5 min, A:B 92:8, v/v; 20 min, A:B 87:13, v/v; 50 min, A:B 85:15, v/v; 70 min, A:B 80:20, v/v; 85 min, A:B 0:100, v/v; then back to initial composition in 2 min and held another 5 min for column re-equilibration. The column temperature was maintained at 35 °C. The flow rate was set at 0.7 mL/min with a split ratio of 25% entering the mass spectrometer.

IT-TOF detection (Shimadzu, Japan) equipped with an electrospray ionization source (ESI) was performed in positive ion mode using the optimized conditions: detector voltage, 1.60 kV; nebulizing gas (N_2) flow, 1.5 L/min; drying gas (N_2) flow, 200 kPa; ion accumulated time, 30 ms; collision energy set at 40% both for MS^2 and MS^3; scan range *m/z* 100–1000 for MS^1, 100–500 for MS^2 and MS^3.

The MDF was performed by MetID solution 1.0, and Shimadzu's Composition Formula Predictor software was used to provide chemical formula for both the precursor and product ions.

Results and discussion

Optimum conditions for LC/MS-IT-TOF analysis

The substances under investigation are alkaloids with a basic nitrogen atom, which makes them predestined for ESI in positive ion mode. MS conditions were optimized on an LC/MS-IT-TOF instrument using the standard solutions of strychnine and brucine (0.1 mg/mL). Solvent effects were studied by on-line mixing of different mobile phases (100 μL/min) with the above solutions (10 μL/min) during continuous infusion. Three different solvents, including water–methanol (85:15, v/v), water–methanol–formic acid (85:15:0.075, v/v/v), and water–methanol–formic acid–ammonium acetate (85:15:0.075, v/v/v, containing 10 mM of ammonium acetate) were compared. It was found that modified solvents provided better ionization in ESI^+ mode. For both of the strychnine and brucine, $[M+H]^+$ ions were commonly detected with high sensitivity (<1 ng/mL) under the water–methanol–formic acid–ammonium acetate solvent condition.

For the purpose of getting the optimized collision energy (CE) that generates available fragment information for structural elucidation and characterization, we performed MS/MS experiments at different CE (10–100%). By gradually increasing the CE, the intensity of product ions was first increased to maximum and then gradually decreased. Even though the optimum CE might vary for different SAs, our study showed that 40% CE is sufficient to cause abundant fragment ions for structural elucidation.

The chromatographic conditions were optimized through several trials to achieve the desired separation, run time and symmetric peak shapes for the metabolites of SAs. We selected the mobile phase consists of water (10 mM ammonium acetate, pH3.0) and methanol as the optimal composition of mobile phase to carry on the process of optimization of HPLC conditions. By the optimal gradient elution, most of the peaks could be separated within 70 min (Fig. 1).

Mass spectral fragmentation of strychnine and brucine in ESI positive mode

A prerequisite for the metabolite identification studies was to record the LC-MS^n spectra of the parent compounds. As the explanations in the literature on the fragmentation patterns of strychnine are quite different from one piece of work to another (Choi *et al*., 2004; Stahl *et al*., 2004; Yan *et al*., 2006), we decided to conduct first a detailed fragmentation study by high-resolution LC/MS-IT-TOF with strychnine and brucine.

In the ESI^+-MS spectrum, the strychnine was observed as a protonated molecule $[M+H]^+$ ion at *m/z* 335.1754. MS/MS analysis of the $[M+H]^+$ ion showed a predominant fragment ion at *m/z* 264.1022 ($[C_{17}H_{14}NO_2]^+$, 1.14 ppm), together with minor ions at *m/z* 307.1450 ($[C_{19}H_{19}N_2O_2]^+$, 2.93 ppm). As illustrated in Fig. 2 (a), the *m/z* 307.1450 could be formed by partial loss of the nitrogen bridge (loss of C_2H_4 at C_{17}–C_{18}) through cleavage at C_7 and C_{17}, N_{19} and C_{18}, and hydrogen transfer from C_8 to N_{19}. The ion at *m/z* 307.1450 can further, via a neutral loss of C_2H_5N (C_{15}–C_{16}–N_{19}) through rearrangement of the six-membered ring located at C_7, C_8, C_{13}, C_{14}, C_{15} and C_{16}, form the base peak at *m/z* 264.1022. To obtain further information on the *m/z* 264.1022, the MS^3 spectrum was acquired. There was one major fragment ion at *m/z* 234.0905 ($[C_{16}H_{12}NO]^+$, −3.42 ppm); several fragment ions of significant abundance at *m/z* 222.0916 ($[C_{15}H_{12}NO]^+$, 1.35 ppm), 206.0954 ($[C_{15}H_{12}N]^+$, −4.85 ppm), 194.0968 ($[C_{14}H_{12}N]^+$, 2.06 ppm) and 184.0749 ($[C_{12}H_{10}NO]^+$, −4.35 ppm) and one minor fragment ion at *m/z* 156.0799 ($[C_{11}H_{10}N]^+$, −5.77 ppm). The fragment ions at *m/z* 234.0905 and 222.0916 were presumably formed through ring contraction by elimination of CH_2O (C_{23}–O_{24}) and C_2H_2O (C_{22}–C_{23}–O_{24}) contained in the seven-membered ring, respectively. These two ions can further, via a neutral loss of CO at C_{10}, form the ions at *m/z* 206.0954 and 194.0968. In another fragmentation pathway, the seven-membered ring was shed off to become the ion at *m/z* 184.0749, with further peak appearing at *m/z* 156.0799 produced by the neutral loss of CO at C_{10}.

Strychnine and brucine show a very similar fragmentation pattern since brucine contains only two additional methoxyl

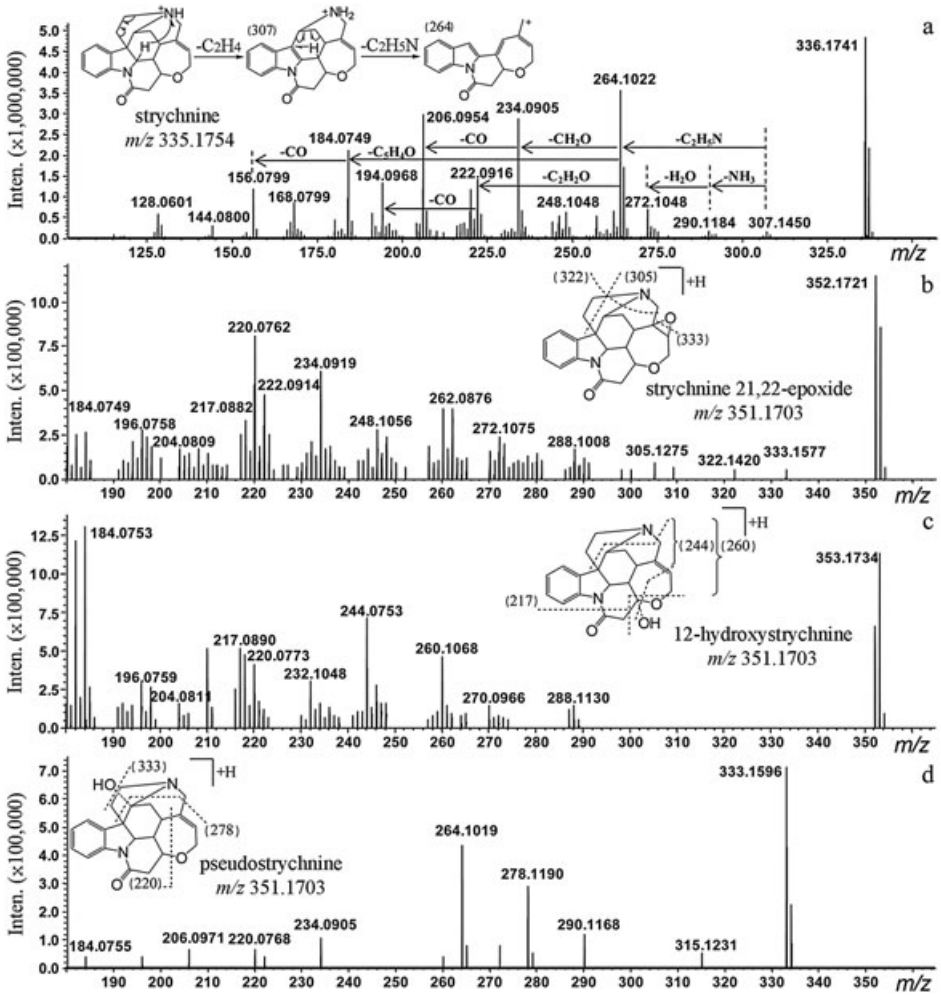

Figure 2. MS/MS spectra of (a) strychnine and (b–d) the metabolites of strychnine. The numbers in brackets indicate the mass to charge ratio of the corresponding fragments.

groups (Fig. 3a). Therefore, most fragments found for strychnine were also detected for brucine, considering a mass shift by 60 Da. Nevertheless, the fragment ion *m/z* 263.0939 ($[C_{17}H_{13}NO_2]^{+\cdot}$, −0.76 ppm) was only observed in the ESI^+-MS/MS spectrum of brucine. The mass difference between the $[M - C_2H_4 - C_2H_5N - CH_2O + H]^+$ ion (*m/z* 294.1123, −0.68 ppm) and the fragment ion *m/z* 263.0941 was 31.0184 Da, indicating the loss of a methoxyl ($CH_3O\cdot$) radical, which could be explained by the presence of the methoxyl groups connected to the benzene ring.

In summary, the protonation of N_{19} atom induces the combined cleavage of nitrogen bridges and seven-membered oxygen-containing ring through successive induction and hydrogen rearrangement effects. These mass spectral fragmentation patterns of strychnine and brucine have provided guidance in the subsequent structure elucidation of their metabolites.

Metabolism of strychnine and brucine in rat liver microsomes

We used the MetID data-processing software utilizing MDF technique to identify metabolite ions. The key to the creation of MDF algorithm was the realization that the mass defects (the nonintegral portion of an *m/z* value) of metabolite ions typically fall within ±50 mDa relative to that of the parent drug. In this study, protonated strychnine ($[C_{21}H_{23}N_2O_2]^+$, mass defect 0.1754 Da) and brucine ($[C_{23}H_{27}N_2O_4]^+$, mass defect 0.1965 Da) were assigned as the filter references. Subsequently, post-run chromatograms are generated in the fixed, narrow mass defect ranges (0.125–0.225 Da for strychnine and 0.146–0.246 Da for brucine), yielding peaks selectively for the drug-related metabolites, and excluding non-metabolite matrix components.

Figure 1 shows the extracted ion chromatograms of $[M + H]^+$ ions of the potential metabolites with the aid of MetID solution software. The facile identification of potential metabolites subsequently enables the execution of MS^n experiments to establish their identities. The assignment of the structures for these metabolites was as follows.

Screening for strychnine metabolites

Metabolites M1–M8. In the full-scan mass spectrum, metabolites M1–M8 were all observed as protonated molecular ions $[M + H]^+$ at *m/z* 351.1703 ($[C_{21}H_{23}N_2O_3]^+$), suggesting that these metabolites were isomers of mono-oxidized metabolites of strychnine.

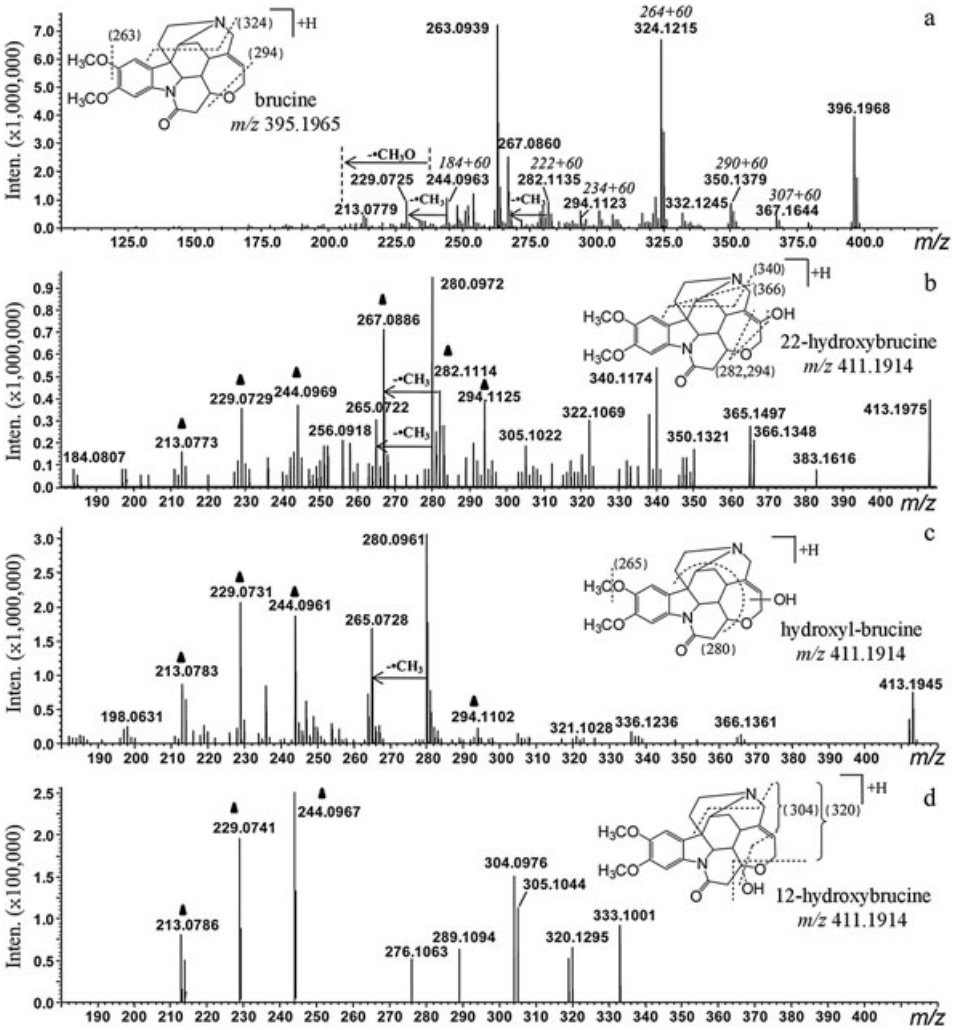

Figure 3. MS/MS spectra of (a) brucine and (b–d) the metabolites of brucine. The numbers in brackets indicate the mass to charge ratio of the corresponding fragments.

For strychnine and its metabolite M1, MS/MS fragmentation patterns of $[M+H]^+$ ions were very similar (Fig. 2a, b). The fragments obtained at *m/z* 272.1075, 248.1056, 234.0919, 222.0914, 220.0762 and 184.0749 were also observed in the spectrum of strychnine, which suggests that the indole ring and lactam moiety remain unchanged. However, a mass difference of 2 Da could be observed for some other fragments (*m/z* 307 → 305, 290 → 288 and 264 → 262). This was due to the C–C double bond formed by H_2O elimination at seven-membered ring, indicating that the double bond at C_{21-22} was epoxidated. In addition, the cleavage of the C_{20-21} bond was observed in the MS/MS spectrum of M1 (*m/z* 322.1420), confirming the presence of a 21,22-epoxide in its structure. Therefore, M1 was identified to be strychnine 21,22-epoxide.

In the MS^2 spectrum of M4 (Fig. 2c), the $[M+H]^+$ at *m/z* 351.1703 produced three characteristic ions at *m/z* 260.1068, 244.0753 and 217.0890, corresponding to the elimination of $C_3H_9NO_2$, $C_4H_{13}NO_2$ and $C_5H_{12}NO_3$, respectively. The fragmentation pathway to form these ions possibly involved two steps: first, eliminating the nitrogen bridges, and then by cleavage at C_{12} to lose different parts of the six or seven-membered ring. It can be concluded that the hydroxyl group which altered the fragmentation pattern of strychnine occurred at the C_{12} position. M4, therefore, was confirmed as 12-hydroxystrychnine.

The product ion mass spectrum of metabolite M5 contained the same fragments of strychnine at *m/z* 290.1168, 264.1019, 234.0905, 206.0971 and 184.0755 (Fig. 2d), which indicated that the oxidation did not occur at any carbon among C_{1-14} and C_{21-23} of the basic skeleton. The loss of water from the protonated molecule ion formed the predominant peak at *m/z* 333.1596, suggesting the presence of a hydroxyl group. The fragment ion at *m/z* 278.1190 (cleavage between C_{20} and C_{21}, C_{16} and C_{19}, C_7 and C_{17}) narrowed down the hydroxylation site to be C_{16}. Based on these results, M5 was confirmed as pseudostrychnine (16-hydroxystrychnine).

Metabolites M3 and M6 gave rise to ions at *m/z* 323.1390, 280.0968, 250.0863, 238.0863 and 200.0706 (theoretical values), which were all 16 Da higher than the corresponding fragments of strychnine, suggesting that the biotransformation might be an addition of a hydroxyl group on the benzene ring. The short retention time of M3 indicated that this metabolite was more hydrophilic than M6. Therefore, the structure of M3 was assigned to be 2-hydroxystrychnine. M6 might be 1-hydroxystrychnine, 3-hydroxystrychnine or 4-hydroxystrychnine; however, 3-hydroxystrychnine was the most likely metabolite under the considerations of electronic effect and steric hindrance.

In the case of metabolite M7, MS/MS resulted in the immediate loss of 17 Da corresponding to an ·OH radical to form *m/z* 334.1667 ($[C_{21}H_{22}N_2O_2]^{+\cdot}$). This was followed by a further elimination of C_2H_4 (*m/z* 306.1368, $[C_{19}H_{18}N_2O_2]^{+\cdot}$), CH_3N (*m/z* 277.1101, $[C_{18}H_{15}NO_2]^{+\cdot}$) and C_3H_5O (*m/z* 220.0759, $[C_{15}H_{10}NO]^+$) groups in one fragment pathway or C_2H_4 and CH_3NO (*m/z* 261.1146, $[C_{18}H_{15}NO]^{+\cdot}$) groups in another fragment pathway, which suggested that the nitrogen atom on the nitrogen bridge was oxidized. M7 was then identified to be strychnine-*N*-oxide.

According to the product ion information obtained from the MS^n spectra of M2 and M8, both of them were mono-hydroxylated metabolites, generated from hydroxyl substitution on the seven-membered ring of strychnine. However, the exact position of hydroxylation could not be characterized.

Metabolites M9–M16. Metabolites M9–M16 were calculated as $C_{21}H_{22}N_2O_4$ by the Formula Predictor software according to the accurate mass measurements. All of them showed a protonated molecule ion at *m/z* 367.1652, 32 Da higher than *m/z* 335.1754, suggesting that they were sequential oxidation (2 × oxidation) metabolites of strychnine.

The MS^2 spectra of the $[M+H]^+$ ions of metabolites M9, M12, M13 and M15 had base peaks at *m/z* 350.1625 formed by the loss of an ·OH group, which were consistent with the N_{19}-oxidation. In the MS^2 spectrum of M9, low abundance ions were observed at *m/z* 335.1395 ($[C_{20}H_{19}N_2O_3]^+$, 1.49 ppm), 321.1608 ($[C_{20}H_{21}N_2O_2]^+$, 3.11 ppm) and 294.1136 ($[C_{18}H_{16}NO_3]^+$, 3.74 ppm) corresponding to the cleavage of the C_{20-21} bond (Fig. 4). This gave support to the presence of a 21,22-epoxide substitution. Therefore, M9 was identified as strychnine 21,22-epoxide-*N*-oxide. M12 and M15 fragmented in a similar way to M7 and were confirmed as the hydroxylated metabolites of strychnine-*N*-oxide. On the basis of the elemental compositions of product ions and bond connectivities present in the strychnine-*N*-oxide, the most likely hydroxylation site was located at the C_2 or C_3. We observed that M12 was more hydrophilic than M15 according to their LC retention time. Thus, M12 and M15 were tentatively identified as 2-OH-strychnine-*N*-oxide and 3-OH-strychnine-*N*-oxide, respectively, with respect to electronic effect.

For metabolites M10, M14 and M16, the mass spectra exhibited identical base fragment ions at *m/z* 349.1547 ($[M+H-H_2O]^+$), together with minor ions at *m/z* 350.1625 ($[M+H-OH]^{+\cdot}$), suggesting that hydroxylation occurs on the seven-membered ring or C_{16} position of the strychnine-*N*-oxide, but the site could not be exactly determined. Product ions for the metabolite M11 were detected at a lower level and thus no structural assignment could be suggested.

Metabolites M17 and M18. Both M17 and M18 showed the protonated molecule ion $[M+H]^+$ at *m/z* 353.1860, and were calculated as $C_{21}H_{24}N_2O_3$ by the Formula Predictor software according to their accurate masses. Thus, M17 and M18 were preliminarily concluded to be the hydrolysis products of strychnine. However, they exhibited remarkably different MS fragmentation patterns. In the case of metabolite M17, the fragment ions at *m/z* 222.0922 and 184.0753 (base peak), identical to strychnine, indicated an unchanged lactam ring and that hydrolysis reaction had not occurred on the amide bond. Other low-abundance product ions were all formed by the cleavage of the C_{20-21} bond, and this confirmed the hydrolysis site to be on the C_{21-22} double bond. Considering the steric hindrance, M17

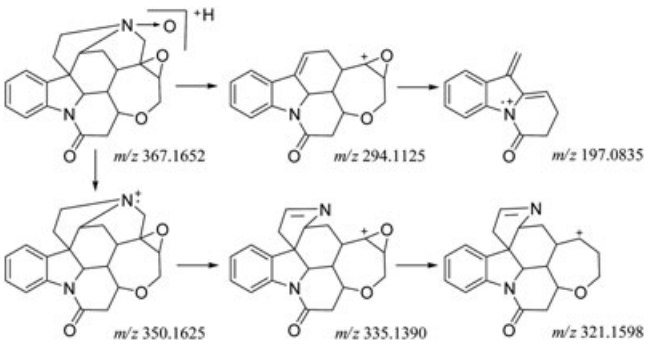

Figure 4. Fragmentation pathway of M9 in positive electrospray ionization mode.

Table 1. LC/MS^2 data of metabolites of SAs after incubation with rat liver microsomes and NADPH

Parent compound	Metabolites	Precursor $[M+H]^+$	Retention time (min)	MS^2 data (percentage base peak, ppm[a])	Identification	Reference.
Strychnine	M1	351.1703	22.42	333.1577 (1.90, −6.30), 322.1420 (2.14, −5.59), 305.1275 (5.88, −3.28), 288.1008 (21.64, −3.82), 272.1075 (35.67, 1.84), 262.0876 (40.06, 4.96), 234.0919 (76.29, 2.56), 222.0914 (50.48, 0.45), 220.0762 (90.70, 2.27), 184.0749 (33.17, −4.35).	Strychnine 21,22-epoxide	Mishima *et al.* (1985); Tanimoto *et al.* (1990)
	M2	351.1703	23.61	220.0751 (100.00, −2.73), 194.0595 (19.21, −2.58), 184.0757 (81.27, 0.00).	Hydroxyl-strychnine	
	M3	351.1703	24.89	280.0961 (100.00, −2.50), 250.0858 (53.67, −2.00), 238.0863 (36.81, 0.00), 222.0924 (37.76, 4.95), 200.0703 (56.01, −1.50), 196.0749 (4.01, −4.08).	2-Hydroxystrychnine	Mishima *et al.* (1985) ; Tanimoto *et al.* (1990)
	M4	351.1703	28.09	260.1068 (40.33, −0.77), 244.0753 (47.99, −1.64), 217.0890 (37.16, 1.84), 210.0920 (41.46, 3.33), 184.0753 (100.00, −2.17), 182.0966 (89.12, 1.10).	12-Hydroxystrychnine	
	M5	351.1703	37.47	333.1596 (100.00, −0.60), 290.1168 (12.09, −2.76), 278.1190 (40.25, 5.03), 264.1019 (62.04, 0.00), 234.0905 (10.18, −3.42), 220.0768 (8.01, 5.00), 206.0954 (8.57, −4.85), 184.0755 (4.82, −1.09).	Pseudostrychnine (16-hydroxystrychnine)	Tanimoto *et al.* (1990)
	M6	351.1703	38.84	323.1363 (6.66, −8.36), 280.0968 (57.59, 0.00), 250.0867 (100.00, 1.60), 238.0863 (34.56, 0.00), 222.0912 (82.66, −0.45), 200.0707 (48.97, 0.50).	3-Hydroxystrychnine	
	M7	351.1703	40.72	334.1667 (100.00, −2.69), 319.1426 (15.67, −4.70), 306.1368 (45.46, 1.63), 291.1249 (9.69, −1.72), 277.1101 (17.76, 1.44), 261.1146 (19.63, −0.77), 233.0831 (17.53, −1.72), 220.0759 (80.07, 0.91).	Strychnine-*N*-oxide	Mishima *et al.* (1985); Tanimoto *et al.* (1990)
	M8	351.1703	42.17	333.1588 (100.00, −3.00), 260.0964 (0.50, 7.69), 210.0917 (1.86, 1.90), 182.0957 (0.44, −3.84).	Hydroxyl-strychnine	
	M9	367.1652	28.83	350.1620 (100.00, −1.43), 349.1539 (14.40, −2.29), 335.1395 (16.99, 1.49), 321.1608 (31.23, 3.11), 307.1444 (13.52, 0.98), 294.1136 (33.85, 3.74), 220.0744 (3.14, −5.91), 197.0830 (12.93, −2.54).	Strychnine 21,22-epoxide-*N*-oxide	
	M10	367.1652	30.24	350.1620 (50.73, −1.43), 349.1547 (100.00, 0.00), 321.1578 (7.32, −6.23).	Hydroxyl-strychnine-*N*-oxide	
	M11	367.1652	32.57	200.0687 (100.00, −9.50), 198.0917 (80.00, 2.02).	2 × Oxidation	
	M12	367.1652	34.15	350.1631 (100.00, 1.71), 322.1325 (15.37, 4.04), 236.0702 (11.92, −1.69), 183.0680 (8.07, 0.55).	2-OH-strychnine-*N*-oxide	
	M13	367.1652	36.68	350.1620 (100.00, −1.43).	Metabolites of M7	
	M14	367.1652	40.12	350.1623 (20.29, −0.57), 349.1537 (100.00, −2.86).	Hydroxyl-strychnine-*N*-oxide	
	M15	367.1652	45.02	350.1637 (100.00, 3.43), 322.1327 (60.91, 4.66), 236.0726 (5.79, 8.47).	3-OH-strychnine-*N*-oxide	

(Continues)

Table 1. *(Continued)*

Parent compound	Metabolites	Precursor $[M+H]^+$	Retention time (min)	MS^2 data (percentage base peak, ppm[a])	Identification	Reference.
	M16	367.1652	65.38	350.1616 (11.79, −2.57), 349.1543 (100.00, −1.15).	Hydroxyl-strychnine-*N*-oxide	
	M17	353.1860	25.43	262.1223 (5.61, −1.14), 246.0927 (11.18, 5.69), 234.0923 (4.29, 4.27), 222.0922 (10.87, 4.05), 184.0753 (100.00, −2.17).	21-Hydro-22-hydroxystrychnine	
	M18	353.1860	40.81	335.1757 (100.00, 0.90), 307.1447 (17.68, 1.95), 221.0834 (5.97, −0.45).	Hydrolysis metabolite	
	M19	333.1598	37.88	—	Dehydrostrychnine	Mishima *et al.* (1985)
	M20	333.1598	42.52	—	Dehydrostrychnine	
	M21	365.1860	37.88	—	Methylation + oxidation	
	M22	365.1860	48.93	—	Methylation + oxidation	
Brucine	M1′	381.1809	26.30	366.1578 (44.36, 1.09), 353.1488 (5.48, −2.27), 336.1224 (11.40, −1.79), 310.1067 (100.00, −2.26), 248.0711 (84.54, 2.02), 236.0705 (47.52, −0.42), 220.0758 (51.06, 0.45).	2-OH-3-methoxystrychnine	
	M2′	381.1809	35.42	366.1560 (5.85, −3.82), 353.1485 (1.70, −3.11), 336.1233 (6.88, 0.89), 310.1076 (100.00, 0.64), 248.0707 (68.07, 0.40), 236.0694 (39.74, −5.08), 220.0746 (22.72, −5.00).	3-OH-2-methoxystrychnine	
	M3′	411.1914	30.91	383.1616 (3.03, 3.91), 366.1348 (27.48, 3.28), 365.1497 (37.58, 0.27), 340.1174 (69.74, −1.47), 322.1069 (40.03, −1.55), 294.1125 (48.21, 0.00), 282.1114 (50.93, −3.90), 280.0972 (100.00, 1.43), 267.0886 (96.87, −1.50), 265.0722 (38.03, −4.15), 244.0969 (49.20, 0.41), 229.0729 (45.90, −1.75), 213.0773 (21.91, −5.16).	22-Hydroxybrucine	
	M4′	411.1914	33.74	280.0961 (100.00, −2.50), 265.0728 (61.45, −1.89), 244.0961 (63.53, −2.87), 229.0731 (65.47, −0.87), 213.0783 (29.18, −0.47).	Hydroxyl-brucine	
	M5′	411.1914	42.67	320.1295 (38.96, 4.37), 304.0976 (79.03, 2.63), 244.0967 (100.00, −0.41), 229.0741 (93.37, 3.49), 213.0786 (42.31, 0.94).	12-Hydroxybrucine	
	M6′	411.1914	55.63	394.1876 (100.00, −2.79), 379.1647 (4.07, −1.32).	Brucine-*N*-oxide	
	M7′	411.1914	58.65	393.1809 (100.00, 0.00).	Hydroxyl-brucine	
	M8′	427.1864	37.21	410.1837 (100.00, 0.24), 395.1586 (3.82, −3.80).	1-OH-brucine-*N*-oxide or 4-OH-brucine-*N*-oxide	
	M9′	365.1860	48.54	350.1614 (7.62, −3.14), 294.1118 (100.00, −2.38), 264.1027 (45.00, 3.03), 252.1023 (27.23, 1.59), 214.0867 (44.63, 1.87).	α-Colubrine or β-colubrine	

[a]Differences between the observed and theoretical values.

was characterized as 21-hydro-22-hydroxystrychnine. In contrast, fragmentation of M18 was highlighted by water loss and the formation of $[M+H-H_2O-C_2H_4]^+$ characteristic fragment, but the position of hydrolysis site could not be exactly characterized.

Metabolites M19–M22. The protonated molecule ion at *m/z* 333.1598 ($[C_{21}H_{21}N_2O_2]^+$) was 2 Da less than *m/z* 335.1754, indicating that both M19 and M20 were the dehydrogenation products of strychnine. M21 and M22 showed the predominant quasimolecular ion $[M+H]^+$ at *m/z* 365.1860 ($[C_{22}H_{25}N_2O_3]^+$), which is a CH_2O more than the parent compound, suggesting that both methylation and oxidation reactions had occurred in this metabolic process. However, these four metabolites could not be further studied by MS^n owing to their too low concentration and thus no exactly structural assignment could be suggested.

Based on the above analysis, 22 metabolites of strychnine were characterized as summarized in Table 1. Incubation with rat liver microsomes in the presence of NADPH gave hydroxylation (M2–6 and M8) as the major pathway of strychnine metabolism, with additional metabolites resulting from N_{19}-oxidation (M7), epoxidation (M1), hydrolysis (M17 and M18), methylation and oxidation (M21 and M22), dehydrogenation (M19 and M20) and combinations thereof (M9–16).

Screening for brucine metabolites

Metabolism of brucine was investigated in rat liver microsomes with appropriate controls, using standard metabolism protocols. Possible metabolite structures were considered based on the structure of brucine and known common metabolic pathways.

In the MS^2 spectra of the $[M+H]^+$ ions at *m/z* 381.1809 from M1′ and M2′, a mass shift of 46 Da could be observed for the major fragments compared with strychnine. This indicated that both M1′ and M2′ were the demethylation products of brucine. There are two methyl groups, the C_2 and C_3 methoxyl groups in brucine, which can be demethylated by cytochrome P450 in rat liver microsomes. According to the elution order on RP-C_{18} column, the demethylation sites of M1′ and M2′ were located at C_2 and C_3, respectively. The proposed fragmentation pathways of M1′ (2-OH-3-methoxystrychnine) are shown in Fig. 5.

Mass spectra of M3′, M4′ and M5′ show the $[M+H]^+$ ions at *m/z* 411.1914, which gave a molecular formula of suggesting the apposition of an O atom. In the MS^2 experiment, most low mass fragments found for M3′, M4′ and M5′ (marked with triangles in Fig. 3b–d) were also detected in the spectrum of brucine, which suggests that the benzene ring remains unchanged. Meanwhile, the product ions in the zone of *m/z* 280–390 of these isomeric metabolites varied remarkably (Fig. 3b–d), and could be used for their differentiation. In the case of M3′ (Fig. 3b), the observed fragments at *m/z* 383.1616 (367 + 16 Da), 366.1348 (350 + 16 Da) and 340.1174 (324 + 16 Da) clearly suggest hydroxylation at C_{22} of the seven-membered ring. Thus, we can conclude that M3′ is 22-hydroxybrucine. On the contrary, no characteristic fragments were detected in MS/MS spectrum of M4′ from *m/z* 294 (Fig. 3c). During the fragmentation to produce ion *m/z* 280.0968 (theoretical value, loss of the C_{17-23}, N_{19} and O_{24} moiety), alternative pathways were available for M3′, but not M4′, to produce *m/z* 282.1114 (222 + 60 Da) and 340.1174 (loss of the nitrogen bridges). The above information implies that M4′ has a hydroxylation substituent at either position C_{13} or C_{14}, but the site could not be exactly determined. For M5′ (Fig. 3d), the presence of the major fragments of *m/z* 320.1295 (260 + 60 Da), 304.0976 (244 + 60 Da, base peak) and 244.0967 (184 + 60 Da) suggested that the hydroxylation took place at the C_{12} in a manner similar to that observed in the formation of M4. Therefore, M5′ was assigned to 12-hydroxybrucine.

Metabolite M6′ was calculated as $C_{23}H_{26}N_2O_5$ by the Formula Predictor software according to the accurate mass measurement.

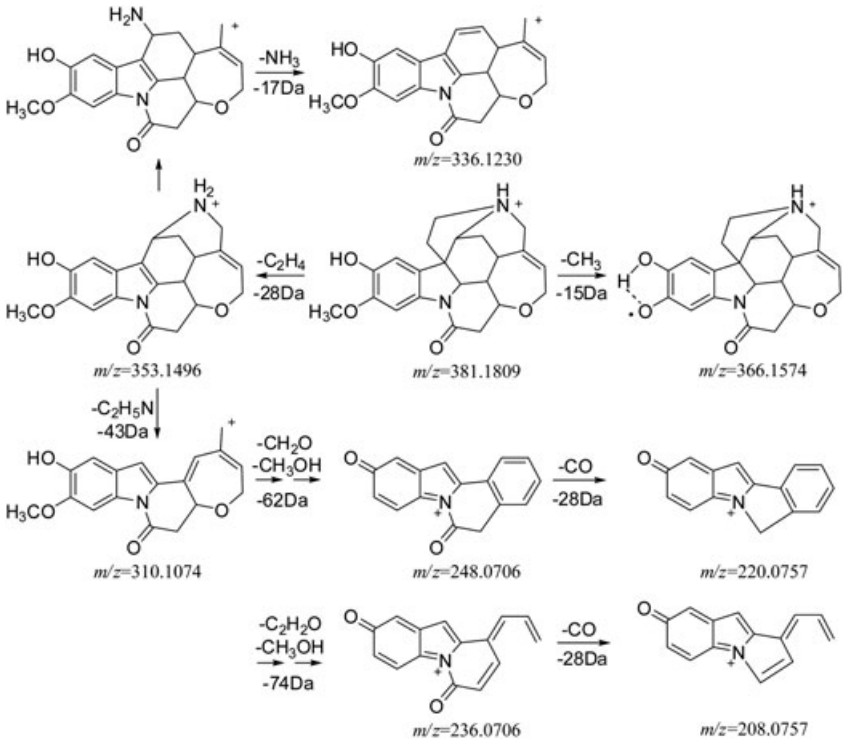

Figure 5. Proposed fragmentation mechanism of the protonated 2-OH-3-methoxystrychnine.

The spectrum of MS^2 obtained from the precursor ion at *m/z* 411.1914 showed two major product ions at *m/z* 394.1876 ($[M+H-OH]^{+\cdot}$, base peak) and 379.1647 ($[M+H-OH-CH_3]^+$), which were 60 Da higher than those of strychnine-*N*-oxide. This indicated that *N*-oxidation, the same as M7 of strychnine, occurred on the N_{19} position. Therefore, M6′ was assigned as brucine-*N*-oxide. In the case of M8′, the protonated molecule ion at *m/z* 427.1864 ($[C_{23}H_{27}N_2O_6]^+$) and its MS^2 ions at *m/z* 410.1837, 395.1586 were all 16 Da higher than those of brucine-*N*-oxide (M6′), respectively. It was thus obvious that M8′ was the hydroxylated product of M6′ at either position C_1 or C_4 on the benzene ring. If the oxidation took place at the C_{7-23}, there should be a corresponding fragment ion of $[M+H-H_2O]^+$ at first, just like the case of metabolite M7′ (Table 1).

M9′ showed the predominant protonated molecule ion at *m/z* 365.1860 that is a CH_2O less than the parent compound brucine, suggesting that it was a de-methoxylation product of brucine. In addition, its MS^2 ions at *m/z* 294.1118, 264.1027, 252.1023 and 214.0867 were 30 Da higher than those of strychnine, respectively. These fragments further confirmed the reliability of the inference above. Therefore, M9′ was identified to be α-colubrine (3-methoxystrychnine) or β-colubrine (2-methoxystrychnine).

As a result, in addition to the unchanged brucine, a total of nine metabolites were found and details are summarized in Table 1. The major biotransformation included hydroxylation (M3′, M4′, M5′and M7′), N_{19}-oxidation (M6′), *O*-demethylation (M1′ and M2′), de-methoxylation (M9′), as well as sequential oxidation (M8′).

Conclusions

By combining the use of the mass defect filters with multistage fragmentations and accurate mass measurements provided by a hybrid ion trap/time-of-flight mass spectrometer, a set of 31 *in vitro* metabolites was identified for the strychnine and brucine. The major biotransformation observed were oxidative processes, including hydroxylation, N_{19}-oxidation, epoxidation, dehydrogenation, as well as methylation and oxidation processes. By comparison, the hydrolysis modification was substantially lower and the *O*-demethylation reaction was only observed in brucine metabolism. The biotransformation sites were subsequently elucidated using their MS^n spectral information and shown to occur within the seven-membered ring, nitrogen bridges and benzene ring moieties. As a result, 26 *in vitro* metabolites, which have not been published to date, were presented in this study. This work will more comprehensively clarify the metabolism characteristics of SAs, and moreover will further improve the *in vivo* metabolism of SAs in animals which plays a key role in drug toxicity evaluation.

Acknowledgments

This work was supported by the Fundamental Research Funds for the Central Universities (program no. JKY2011037).

References

Agrawal SS, Saraswati S, Mathur R and Pandey M. Cytotoxic and antitumor effects of brucine on Ehrlich ascites tumor and human cancer cell line. *Life Sciences* 2011; **89**: 147–158.

Bradford MM. A rapid and sensitive method for the quantification of microgram quantities of protein utilizing the principle of proteindye binding. *Analytical Biochemistry* 1976; **72**: 248–254.

Choi YH, Sohn YM, Kim CY, Oh KY and Kim J. Analysis of strychnine from detoxified *Strychno nux-vomica* seeds using liquid chromatography–electrospray mass spectrometry. *Journal of Ethnopharmacology* 2004; **93**: 109–112.

Deng XK, Yin FZ, Lu XY, Cai BC and Yin W. The apoptotic effect of brucine from the seed of *Strychnos nux-vomica* on human hepatoma cells is mediated via Bcl-2 and Ca^{2+} involved mitochondrial pathway. *Toxicological Sciences* 2006; **91**: 59–69.

Mishima M, Tanimoto Y, Oguri Z and Yoshimura H. Metabolism of strychnine *in vitro*. *Drug Metabolism and Disposition: the biological fate of chemicals* 1985; **13**: 716–721.

Oudhia P. 2008. *Strychnos nux-vomica* L. Record from Protabase, Schmelzer GH and Gurib-Fakim A (eds). PROTA (Plant Resources of Tropical Africa/Ressources végétales de l'Afrique tropicale), Wageningen, Netherlands. Available from: http://database.prota.org/search.htm (accessed 22 October 2011).

Prasad B, Garg A, Takwani H and Singh S. Metabolite identification by liquid chromatography-mass spectrometry. *Trends in Analytical Chemistry* 2011; **30**: 360–387.

Stahl RS, Arjo WM, Wagner KK, Furcolow C, Nolte DL and Johnston JJ. Development of a high performance liquid chromatography/mass spectroscopy method for the determination of strychnine concentrations in insects used to assess potential risks to insectivores. *Journal of Chromatography B* 2004; **811**: 257–262.

Tanimoto Y, Ohkuma T, Oguri K and Yoshimura H. Species difference in metabolism of strychnine with liver microsomes of mice, rats, guinea pigs, rabbits and dogs. *Journal of Pharmacobio-Dynamics* 1990; **13**: 136–141.

Tanimoto Y, Ohkuma T, Oguri K and Yoshimura H. A novel metabolite of strychnine, 22-hydroxystrychnine. *Xenobiotica; the Fate of Foreign Compounds in Biological Systems* 1991; **21**: 395–402.

Wang QW, Liu L and Huang GZ. Study of toxicology of *Strychnos*. *Journal of Forensic Medicine* 2004; **20**: 183–184.

Yan J, Liu ZQ, Yan CY, Xing JP and Liu SY. Analysis of strychnos alkaloids using electrospray ionization Fourier transform ion cyclotron resonance multi-stage tandem mass spectrometry. *Rapid Communications in Mass Spectrometry* 2006; **20**: 1335–1344.

Yin W, Wang TS, Yin FZ and Cai BC. Analgesic and anti-inflammatory properties of brucine and brucine N-oxide extracted from seeds of *Strychnos nux-vomica*. *Journal of Ethnopharmacology* 2003; **88**: 205–214.

Yuan CH, Sun LR, Zhang M, Li SJ, Wang XM, Gao TM and Zhu XH. Inhibition of human $Na_v1.5$ sodium channels by strychnine and its analogs. *Biochemical Pharmacology* 2011; **82**: 350–357.